

Pulsed radiofrequency for chronic pain: *in vitro* evidence of an electroporation mediated calcium uptake

Borja Mercadal^a, Rubén Vicente^b and Antoni Ivorra^{a,c}

^aDepartment of Information and Communication Technologies, Universitat Pompeu Fabra, Roc Boronat, 138, 08018, Barcelona, Spain

^bLaboratory of Molecular Physiology, Experimental and Health Sciences Department, Universitat Pompeu Fabra, Doctor Aiguader, 88, 08003, Barcelona, Spain;

^cSerra Húnter Fellow Programme, Universitat Pompeu Fabra, Barcelona, Spain

Correspondence:

Borja Mercadal

Department of Information and Communication Technologies

Universitat Pompeu Fabra

Address: Roc Boronat, 138, 08018 Barcelona, Spain

Email: borja.mercadal@upf.edu

Phone: +34 93 542 1578

Abstract

Pulsed radiofrequency (PRF) treatments for chronic pain consist in the delivery of a train of sinusoidal electric bursts to the targeted nerve. Despite numerous clinical evidence of its efficiency, the mechanism of action of PRF remains unclear. Since most of the reported biological effects of PRF can be initiated by a calcium influx into the neurons, we hypothesized that PRF may induce a mild electroporation effect causing a calcium uptake. To test this hypothesis, HEK-293 cells were exposed to PRF bursts and cytosolic calcium and Yo-Pro-1 uptake were monitored. After a single burst, calcium peaks were observed for electric fields above 480 V/cm while the uptake of Yo-pro-1 was insignificant. After a train of 120 bursts, the electric fields required to induce a calcium and Yo-pro-1 uptake decreased to 330 V/cm and 880 V/cm respectively. Calcium peaks were not detected when cells were treated in calcium free media. The temperature increase during the treatments was lower than 5 °C in all cases. Finally, the cell response for different burst frequencies and extracellular media conductivities correlated with the induced transmembrane voltage calculated with a numerical model. Our results support the hypothesis of an electroporation mediated calcium influx.

Keywords

Sine waves; Neuropathic pain; Neuromodulation; Cell membrane; Electric fields;

1. Introduction

Pulsed radiofrequency (PRF) treatments consist in the delivery of a train of sinusoidal electrical bursts (5-20 ms length) in the radiofrequency range (500 kHz) at a repetition rate of a few hertz (2-5 Hz). This treatment modality has been applied at various locations along the afferent pain pathways such as directly to the affected nerve [1], adjacent to the dorsal root ganglion [2] or in intra-articular fashion [3] and it proved to be effective in managing pain in patients suffering chronic pain in all cases. Nowadays the most common pathologies where PRF is indicated are radicular pain, trigeminal neuralgia, occipital neuralgia and shoulder and knee pain [4].

PRF originated from conventional thermal radiofrequency as clinical researchers were seeking for a less destructive radiofrequency based treatment to be applied to the afferent nervous pathways [5]. Two decades after its conception and despite multiple evidence of its effectiveness [4], the exact mechanism of action of PRF has not been revealed yet. There is evidence that the analgesic effect of PRF is neither related to thermal effects nor to a permanent physical neural damage [6–9]. Currently most studies suggest that PRF induced pain relief takes place through a neuromodulatory-type process that alters the synaptic transmission or the excitability of C fibers [10–12]. These fibers carry pain and temperature sensations and are involved in most neuropathic pain syndromes [13].

Animal studies have exhibited several biological effects of PRF. Some studies have shown morphological changes in the inner structures of axons [9,14–16]. Other studies have reported molecular effects such as: alterations of cellular activity [17] and gene expression [18–21], an increase in the expression of inflammatory proteins [16] and the inhibition of extracellular signal-regulated kinases [22]. Also, evidence of a long-term depression effect was found in a recent study [23]. These findings have lead to several possible explanations on how PRF inhibits the transmission of pain signals from a biological perspective. However, there has been little progress in elucidating the underlying biophysical mechanisms by which the electric bursts produce these effects.

Interestingly, most of the effects reported after PRF treatments can be triggered by an increase in the cytosolic free calcium (Ca^{2+}) concentration, a second messenger involved in many short and long term cellular processes. This may link PRF effects with a direct effect of the electric fields. We hypothesize that PRF causes a permeabilization of the neural membrane through a mild electroporation process leading to a Ca^{2+} influx. Given that this hypothetical Ca^{2+} increase could occur in the same manner in different parts of the neuron, it would explain the fact that PRF can be effectively applied at different regions of the afferent nervous pathways.

Electroporation is a biophysical phenomenon in which cell membrane permeability to ions and molecules is increased when the cell is briefly exposed to high electric fields [24]. This increase in permeability has been attributed to the formation of nanometric pores in the cell membrane, hence the term electro-poration. Electroporation is typically performed by delivering a series of short (100 μs) DC pulses but it also appears when radiofrequency bursts are delivered [25–27].

In the present study, we have performed a series of *in vitro* experiments and we have used numerical models in order to investigate the possibility that PRF electric fields cause a Ca^{2+} influx into neuronal cells and elucidate the pathways of this influx.

2. Materials and methods

2.1 Cell culture

Human embryonic kidney cells, HEK-293, were grown in Dubelcco's modified Eagle's medium (Gibco, Dublin, Ireland) supplemented with 10% fetal bovine serum (Biosera, Ringmer, East Sussex, UK) and

1% streptomycin/penicillin (Panreac, Barcelona, Spain). Cells were incubated at 37 °C in a humidified environment containing 5% CO₂. The day before performing the experiments, the cells were seeded into 4 well Nunc™ Lab-Tek™ chambered coverslips (Thermofisher, Waltham, MA, USA) and incubated overnight.

2.2 Electric burst delivery

The most common treatment protocol in clinical PRF treatments consists in a train of sinusoidal bursts (500 kHz) with a burst length of 20 ms and delivered at a repetition rate of 2 Hz for a few minutes (see Figure 1a). In this study, cells were exposed to sinusoidal bursts of different frequencies keeping the length of the bursts to 20 ms in all cases. The applied voltages ranged between 50 and 100 V in the experiments where a single burst was applied and between 40 and 70 V in those involving the delivery of several bursts. All treatments were performed at room temperature. The sinusoidal bursts were generated by an AFG3022B function generator (Tektronix, Beaverton, OR, USA) connected to a WMA-300 high voltage amplifier (Falco Systems, Katwijk aan Zee, The Netherlands). The set-up used to deliver the electric bursts to the cells consisted of an acupuncture needle (shaft diameter of 300 μm) and a stainless steel plate electrode located at the opposite side of the chamber acting as a reference electrode (see Figure 1b Figure). The needle was placed in contact with the bottom of the chamber and parallel to it. Finally, the voltage applied between the needle and the plate was measured by a digital oscilloscope (DSO1014A, Agilent, Santa Clara, CA, USA).

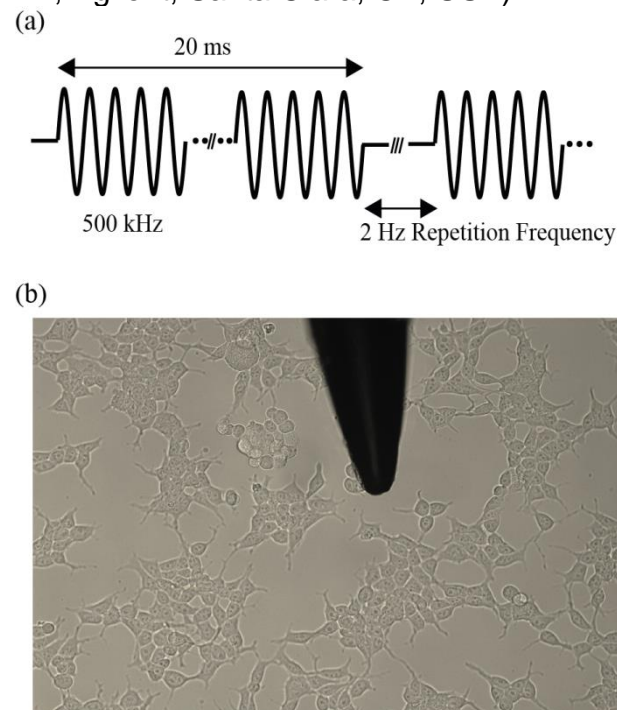


Figure 1: (a) Typical PRF waveform used in the clinical practice (b) Microscopy image of the set-up showing the needle tip and the cells under study.

Typically, in experiments that involve the delivery of pulsed electric fields to cells, researchers use two parallel plates (or wires) in order to generate a relatively uniform and controllable electric field between them. In the present study, however, a different approach was taken in order to reproduce the temperature variations in the tissue during PRF treatments in a clinical setting. It has been shown that during a clinical PRF treatments, the cumulative temperature increase around the electrode, although not irrelevant, is insufficient to create a thermal damage to the tissues [28,29]. However, each burst generates a brief but large temperature spike that can cause a temperature increase of up to a 25 °C at the tip of the electrode. Therefore, the electrode arrangement was chosen aiming to minimize the cumulative temperature increase in the buffer while generating large temperature spikes at each burst.

Unless stated otherwise, the experiments were performed using a physiological buffer consisting of 135 mM NaCl, 5 mM KCl, 2 mM MgCl₂, 10 mM HEPES, 10 mM glucose, 2 mM CaCl₂, (pH 7.4, 310 mOsm, conductivity 1.51 S/m). In the experiments with a Ca²⁺ free extracellular medium, CaCl₂ was replaced by 2 mM EGTA (a Ca²⁺ chelator). When indicated in the text, experiments were performed using a buffer with a low electric conductivity (10 mM NaCl, 250 mM Sucrose, 5 mM KCl, 2 mM MgCl₂, 10 mM HEPES, 10 mM glucose, 2 mM CaCl₂, pH 7.4, 290-310 mOsm, conductivity 0.26 S/m). All these chemicals and reagents were acquired from Panreac.

2.3 Fluorescence labeling and imaging

Intracellular Ca²⁺ concentration was assessed using Calcium Green-1, a dye that exhibits an increase in fluorescence emission upon binding to Ca²⁺. In its acetoxymethyl (AM) ester form, this molecule can passively diffuse into the cell and, once inside, the intracellular esterases cleave the AM group trapping the dye into the cell. To label cells, growth medium was replaced by the physiological buffer and Calcium Green-1 AM (Invitrogen, Carlsbad, CA, USA) was added at a final concentration of 5 μM. Cells were incubated for 40 minutes at 37 °C before being washed thoroughly. Then, the solution was replaced by the desired buffer to perform the experiments.

To assess membrane permeability to larger molecules, growth medium was replaced by the buffer and Yo-Pro-1 (Sigma Aldrich, Saint Louis, MO, USA) was added to a final concentration of 2 μM immediately before the experiments. Yo-pro-1 is a fluorescent molecule that, in normal conditions, cannot enter the cell. It has a high affinity for binding to nucleic acids and when this happens its fluorescence is largely enhanced. For these reasons, among other applications, Yo-Pro-1 is commonly used as a marker to detect electroporation [30].

Images were acquired with a Leica DMI6000B (Leica, Wetzlar, Germany) inverted microscope using a 20x objective. Time series image stacks were captured through the Leica LAS X software. For the assessment of the transient Ca²⁺ response, images were taken every 2 seconds for 30 seconds before the burst delivery and for at least 1 minute after the end of the treatments. When evaluating the uptake of Yo-Pro-1, images were taken every 30 seconds for at least 15 minutes after the treatments.

2.4 Image analysis

The acquired images were processed using Fiji [31] an open source software based on Image J [32]. Regions of interest (ROI) were created for each cell and the average fluorescence was measured for all time points. The average background fluorescence was subtracted to the fluorescence values obtained and the resulting values were converted to $\Delta F/F_0(\%) = 100(F - F_0)/F_0$, where F_0 is the average fluorescence of the ROI before the burst delivery and F is the fluorescence of the ROI at the considered time step.

To analyze the transient Ca²⁺ response to the bursts, the time evolution of $\Delta F/F_0$ was processed in MATLAB (Mathworks Inc, Natick, MA, USA). Cells were classified based on whether or not they exhibited a Ca²⁺ peak. In order to detect Ca²⁺ peaks, the time derivative of the fluorescence was calculated and a threshold was applied to its maximum value. If the maximum of the derivative was above the threshold, first the position of the maximum was checked and only those cases whose maximum took place after the burst were considered. Finally the average fluorescence signal of the 10 following seconds was calculated. Only those peaks whose average was more than 3 times higher than the standard deviation of the signal before the burst delivery were counted. This detection process aimed at minimizing the number of spontaneous Ca²⁺ spikes or image artifacts counted as responses to the bursts.

To detect Yo-Pro-1 uptake, a threshold was applied to the average final fluorescence of each cell in order to decide whether or not the dye was internalized. This threshold was determined as follows: a typical electroporation protocol (8 pulses, 100 μs pulse length) was delivered to our cells and the

fluorescence intensity was measured before the delivery of the pulses and 15 minutes after the delivery. The threshold was calculated as:

$$Thr = F_0 + 0.2(F - F_0) \quad (1)$$

Where F_0 is the average fluorescence of the cells before the delivery of the pulses and F is the average fluorescence of the cells after the delivery of the pulses. The 0.2 factor was chosen to minimize the number of false negatives (i.e. capture cells with a low uptake) but at the same time ensure that the threshold was more than 5 times above the standard deviation of the initial fluorescence.

2.5 Estimation of the electric field exposure for each cell

Our set-up generates a heterogeneous electric field. Thus, in a sample each cell was exposed to a different electric field. The electric field exposure of each individual cell was estimated through finite element modeling. The geometry of our set-up was simulated in COMSOL Multiphysics 4.4 (COMSOL AB, Stockholm, Sweden) by defining an arbitrary 1 V voltage difference between the needle and the plate (See Figure 2). The steady state solution of the problem was calculated by solving the Laplace equation using the electric currents module of COMSOL.

$$\vec{\nabla} \cdot (\sigma \vec{\nabla} V) = 0 \quad (2)$$

Then the results were scaled to the desired voltage to generate electric field maps for each of the applied voltages and extract the electric field exposure of each cell. These electric field values were assigned based on the position of the cells relative to the needle tip. To calculate these relative positions, first, the position of the needle tip was obtained from brightfield images captured before the delivery of the bursts. Second, the position of each cell was calculated by measuring the position of the center of the ROIs. Then, using these two values the relative positions were calculated. Finally, an electric field value was assigned to the ROI by searching for the closest point to the relative position in the electric field maps generated previously.

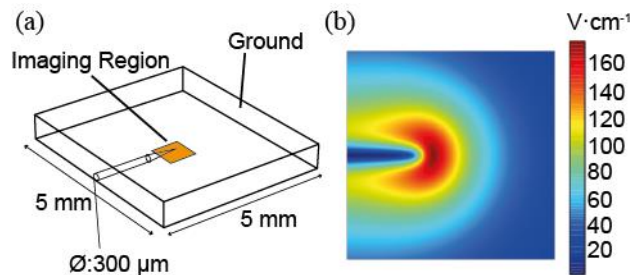


Figure 2: (a) Model geometry. (b) Electric field distribution within the imaging region when a voltage of 10 V is applied between the needle and the plate. Note that the relation between the voltage and the electric field is linear, therefore, the results can be scaled to the different voltages applied in our experiments.

2.6 Statistics

All the processing explained above led to a series of data consisting in an electric field exposure and a binomial response for each cell (either relative to Ca^{2+} or to Yo-pro-1). In order to interpret these data and compare the different treatments, the results were adjusted to a logistic regression:

$$p(E) = \frac{1}{1 + \exp(-(\beta_0 + \beta_1 \cdot E))} \quad (3)$$

Where $p(E)$ is the probability of a cell to show a Ca^{2+} peak as a function of the electric field exposure, E . The values of the parameters β_0 and β_1 were adjusted using the R-3.5.3 software package [33]. For each treatment protocol and conditions at least 15 different experiments were conducted and 40-80 cells were analyzed in each experiment.

2.7 Temperature measurement

Rhodamine B (Sigma Aldrich), a temperature sensitive dye, was used to measure the evolution of the temperature in the medium during the delivery of the electric bursts. The fluorescence of this molecule decreases with temperature [34], and its practically not affected by the external pressure and pH above pH values of 6 [35].

Rhodamine B was dissolved in our buffer to a final concentration of 100 μM and the solution was added into empty chambered coverslips at the same volume used in the experiments with cells. To measure the temperature evolution during the electric treatments, trains of bursts were delivered using the exact same set-up as the experiments explained above. Simultaneously, fluorescence images were taken every 100 ms with a Leica DMI6000B inverted microscope using a 20x objective. The images obtained were analyzed using Image J. At each time point, the average fluorescence in a region close to the needle tip was calculated.

In order to convert the measured fluorescence values to temperature, a calibration procedure was carried out for our set-up. The solution was gradually warmed as follows: two stainless steel plates were placed at opposite sides of the chambered coverslips and were connected to the amplifier. A continuous 500 kHz waveform was generated in order to warm the solution by Joule heating. Images were taken every 15 seconds while simultaneously measuring the temperature using a thermistor. The temperature was increased from room temperature to 50 $^{\circ}\text{C}$ within an approximately 15 minutes time span. This process was repeated in 8 independent experiments. Finally, the acquired fluorescence intensity values as a function of the temperature were used to adjust a second-degree polynomial with the least squares method using the R-3.5.3 software package [33].

2.8 Simulation of the induced transmembrane voltage

The transmembrane voltage (TMV) induced by the electric fields applied in our experiments was calculated by numerical modeling. To do so, realistic 3D geometrical models of the cells were generated from confocal microscopy images. First, for membrane detection, cells were stained for 20 min in ice with 100 $\mu\text{g/ml}$ concanavalin A tetramethylrhodamine (Invitrogen) and then fixed with 4% paraformaldehyde in PBS. Digital images were taken using a Leica TCS SP8 confocal microscope (Leica, Wetzlar, Germany). Cross section images of the cells were obtained by shifting the microscope focus at constant steps (0.3-0.6 μm) from the bottom of the cell to the top. The acquired image stacks were imported to Fiji, and 3D surfaces were constructed using the 3D viewer application of Fiji [36]. Then, these surfaces were smoothed and converted to solid using Meshmixer (Autodesk Inc, San Rafael, CA, USA). Finally, the smoothed surfaces were imported to COMSOL to calculate the induced TMV for different burst frequencies. To do so, the cell membrane was modeled as a surface with the following boundary condition:

$$\vec{n} \cdot \vec{j} = \frac{\sigma_m(V_i - V_o)}{h} + \frac{\varepsilon_m}{h} \frac{\partial(V_i - V_o)}{\partial t} \quad (3)$$

where V_i and V_o are the potentials in the inner and the outer sides of the boundary, σ_m is the membrane conductivity, ε_m is the permittivity of the membrane, and h is membrane thickness. The product $\vec{n} \cdot \vec{j}$ represents the normal current that flows through the membrane. The induced TMV for an arbitrary electric field was calculated by solving the Laplace equation (eq. (2)) using the *Electric currents* module and a frequency domain study. The extracellular conductivity was set to either 1.51 or 0.26 S/m (values measured for our buffers). The rest of the parameters can be found in Table 1.

Symbol	Value	Definition, justification or source
σ_m	2.5×10^{-7} S/m	Membrane conductivity [37]
σ_e	1.51 or 0.26 S/m	Measured values
σ_i	0.5 S/m	Intracellular conductivity[38]

h	5 nm	Membrane thickness[39]
ϵ_e	70	Relative permittivity of the extracellular medium [40]
ϵ_i	70	Relative permittivity of the intracellular medium [40]
ϵ_m	5	Relative permittivity of the membrane [40]

Table 1: Parameters used in the model

3. Results

3.1 Ca²⁺ uptake occurs at lower electric fields than Yo-pro-1 uptake

First of all we exposed the cells to PRF bursts (500 kHz, 20 ms length) and compared the effects of a single burst with the effects of 120 bursts (delivered at a frequency of 2 Hz) in terms of the free cytosolic Ca²⁺ concentration and the uptake of Yo-pro-1. Figure 3a-c show representative examples of the time evolution of the fluorescence in single cells. For convenience, when comparing the different sets of experiments, we will define the E_{50} as the electric field that has a probability of 0.5 to induce a cell response (either a Ca²⁺ peak or Yo-Pro-1 uptake).

The results depicted in Figure 3d show the probability of the cells to display a peak as a function of the electric field according to the logistic regression (Eq. (3)) obtained by fitting the data. After a single burst, the E_{50} to cause a Ca²⁺ peak is 480 V/cm. In contrast, Yo-pro-1 uptake was almost nonexistent after a single burst in the range of electric fields used in our study. When multiple bursts were delivered to the cells, the E_{50} values obtained either for a Ca²⁺ peak or Yo-Pro-1 uptake significantly decreased. In this case, the E_{50} values obtained were around 330 V/cm and 880 V/cm for a Ca²⁺ peak and Yo-Pro-1 uptake respectively.

The same treatments were delivered in the absence of extracellular Ca²⁺ (see Figure 3e) and no changes in cytosolic Ca²⁺ concentration were detected when a single burst was delivered. When multiple bursts were delivered, Ca²⁺ peaks were observed in the cells treated in the Ca²⁺ free media but only at significantly higher electric fields than in normal conditions. In this case the probability of having a Ca²⁺ peak was around 30% for an electric field of 1000 V/cm.

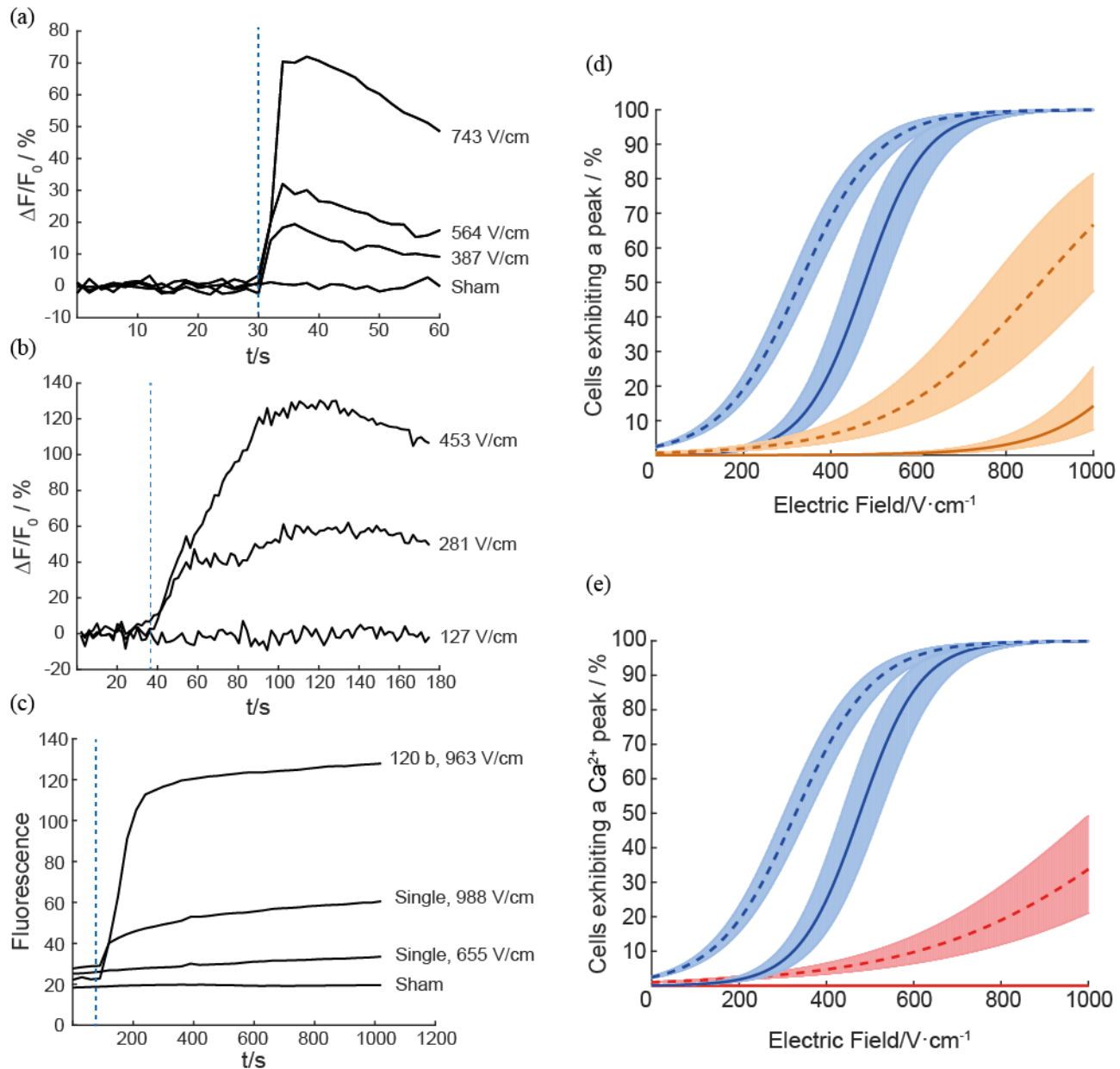


Figure 3: (a) Examples of the time evolution of the Calcium green-1 relative fluorescence change in single cells obtained when a single, 20 ms, PRF burst was delivered. (b) The same as in (a) but when 120 bursts were applied at a repetition rate of 2 Hz. (c) Time evolution of the fluorescence intensity in single cells treated in the presence of Yo-Pro-1 with a single or 120 PRF bursts. The dashed vertical lines show the time at which the treatment was applied. (d) Probability of a cell to exhibit a Ca^{2+} peak (blue) or Yo-Pro-1 uptake (orange) as a function of the electric field as obtained by fitting a logistic regression to our experimental data. Solid lines show the probability when a single burst is applied and dashed lines show the probability when 120 bursts are applied at a repetition rate of 2 Hz. (e) Probability of a cell to exhibit a Ca^{2+} peak as a function of the electric field in normal conditions (blue) and when cells are treated in a Ca^{2+} free medium (red). Solid lines show the probability when a single burst is applied and dashed lines show the probability when 120 bursts are applied at a repetition rate of 2 Hz. The results in (d) and (e) are presented as probability (line) \pm standard error (shaded region).

3.2 The temperature increase was lower than 5 °C

The temperature of the medium during the delivery of successive bursts at a repetition rate of 2 Hz was measured. The fluorescence of Rhodamine B was averaged over two areas, one close to the needle tip and one far from it (see Figure 4a). Figure 4b shows the results obtained within the calibration

process as well as the second-degree polynomial that better fitted with the results. Once the set-up was calibrated the same treatments with multiple bursts as in Figure 3 were applied. Figure 4c-d show the electric field distribution when the lowest and the largest voltage amplitudes are applied in our experiments (40 and 70 V). Figure 4e-f show the temperature evolution over time obtained when bursts with these voltages were applied continuously at a repetition rate of 2 Hz. The cumulative temperature increase did not exceed 4.5 °C in any case. The time evolution of the temperature was very similar on average at the two measured regions. However, significantly larger temperature spikes appeared after each burst in the region close to the needle tip.

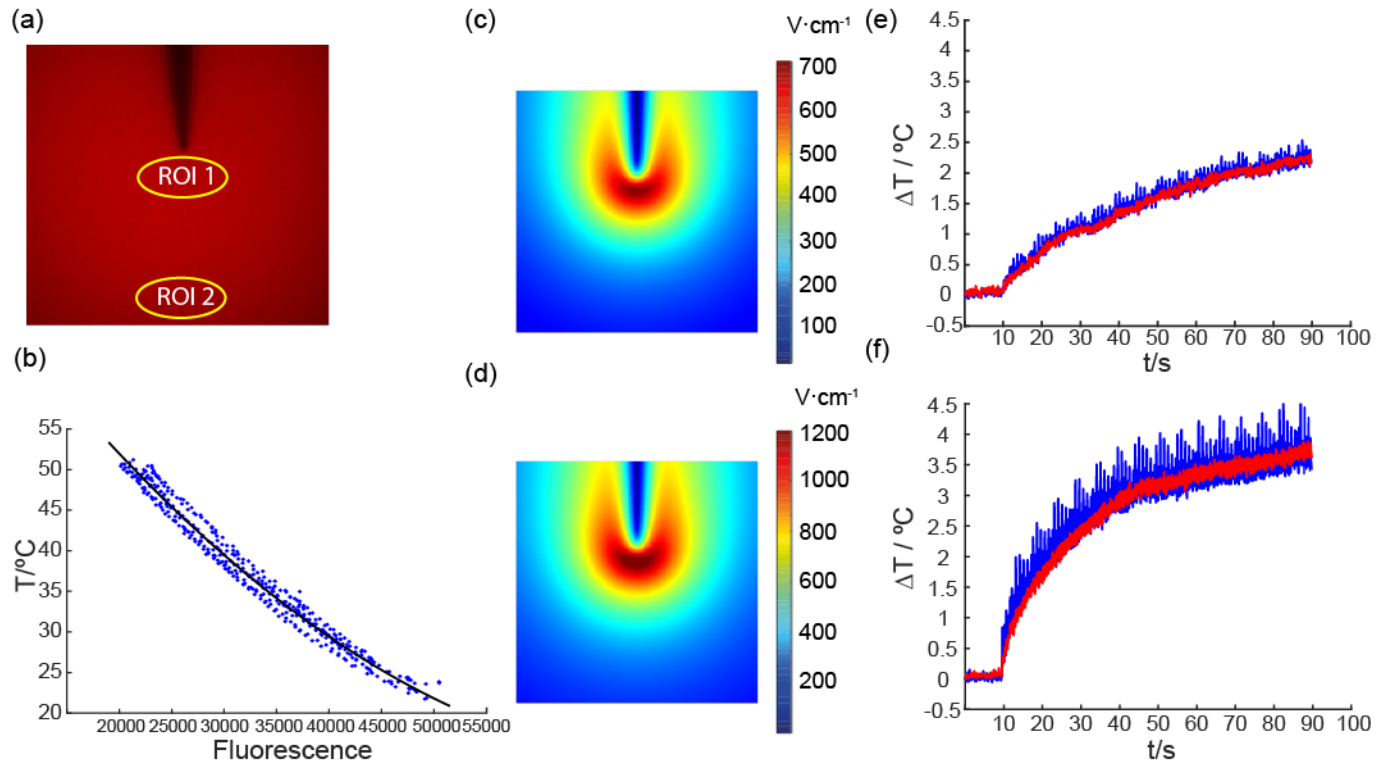


Figure 4: (a) Regions of interest (ROIs) where the fluorescence values were averaged. (b) Temperature as a function of the fluorescence intensity obtained for our set-up during the calibration process and a second-degree polynomial adjusted by the least squares method (black line). The polynomial that best fits the results was: $y = 1.22 \cdot 10^{-8}x^2 - 1.86 \cdot 10^{-3}x + 84.3$ ($R^2=0.98$). (c) Electric field distribution when bursts with an amplitude of 40 V are delivered. (d) Electric field distribution when bursts with an amplitude of 70 V are delivered. (e) Average temperature increase over time in the ROIs shown in (a) (blue: ROI 1, red: ROI 2) when bursts (500 kHz, 20 ms) with an amplitude of 40 V are delivered at 2 Hz. (f) Same as in (e) when bursts (500 kHz, 20 ms) with an amplitude of 70 V are delivered at 2 Hz.

3.3 Ca²⁺ uptake depends on the burst frequency and the medium conductivity

Single bursts with different frequencies but maintaining the burst length at 20 ms were applied. The results, presented in Figure 5a, show a clear dependence of the effects on the frequency. The E_{50} values to induce a Ca²⁺ peak are approximately 400, 480 and 700 V/cm, for 10 kHz, 500 kHz and 2 MHz respectively.

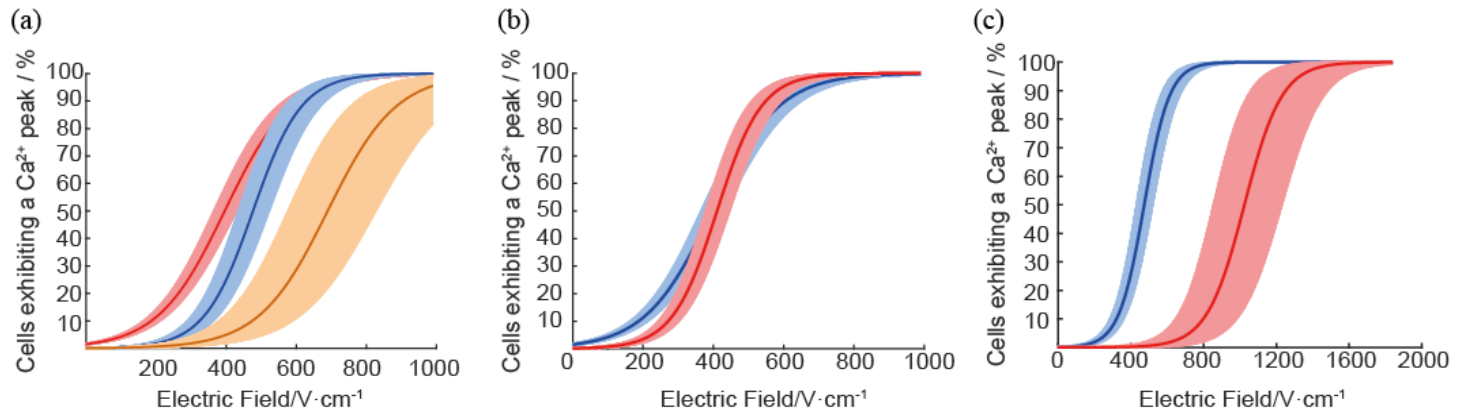


Figure 5: (a) Probability of a cell to exhibit a Ca^{2+} peak as a function of the electric field after the delivery of a single 20 ms burst with a frequency of 10 kHz (red), 500 kHz (blue) or 2 MHz (orange). (b) Probability of a cell to exhibit a Ca^{2+} peak as a function of the electric field when a single 20 ms burst with a frequency of 10 kHz is applied in a medium with an electrical conductivity of 1.51 S/m (blue) or 0.26 S/m (red). (c) Same as (b) but when a single 20 ms burst with a frequency of 500 kHz is applied. All results are presented as the probability function obtained from the logistic regression (line) \pm standard error (shaded region).

The effect of the extracellular medium conductivity was also assessed. Figure 5b-c shows the results obtained by delivering single bursts of frequencies of 10 kHz and 500 kHz using two buffers with different conductivity (1.51 S/m and 0.26 S/m). While the responses are almost identical for 10 kHz regardless of the medium conductivity, a significant difference is observed for 500 kHz. When the cells are treated in the low conductivity buffer, the obtained E_{50} increases to 1020 V/cm for a single 500 kHz burst.

3.4 Numerical results show the same dependence of the induced TMV on frequency and medium conductivity

Finally, we built a realistic geometrical model of our cells in order to calculate the induced TMV in our experiments. The induced TMV was simulated for different frequencies and the two extracellular conductivity values used in our experiments. The results, presented in Figure 6, show a decrease of the TMV with the frequency as expected. However, the induced TMV begins to decrease at lower frequencies when cells are surrounded by the low conductivity extracellular medium. As a consequence the induced TMV is lower in the low conductivity media for high frequencies.

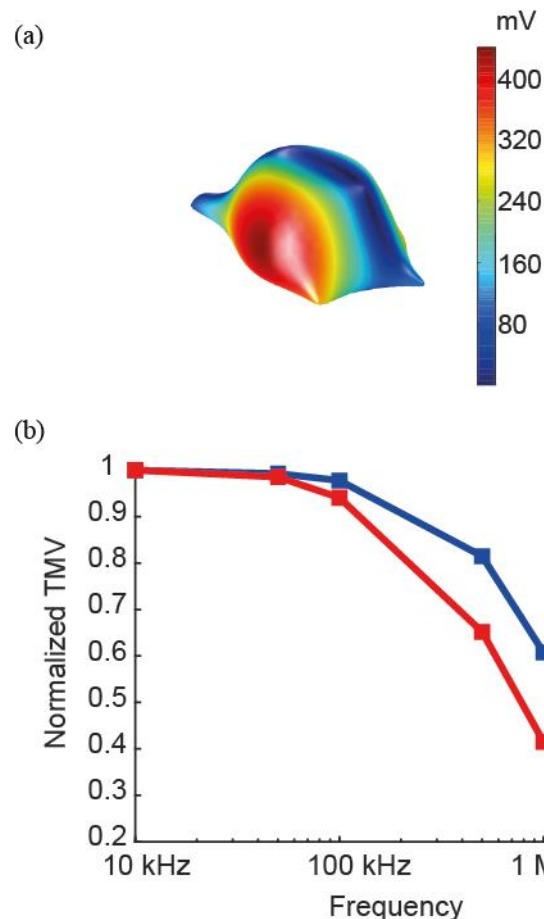


Figure 6: Induced TMV calculated by a FEM model of the cell geometry. The upper image shows the maximum induced TMV amplitude (in mV) when PRF bursts with an electric field amplitude of 400 V/cm are delivered to a HEK cell. The lower plot shows the normalized maximum TMV (with respect to the value at 10 kHz) induced to the cells as a function of the frequency of the bursts when the extracellular conductivity is 1.51 S/m (blue) or 0.26 S/m (red).

4. Discussion

Our results show that the PRF bursts can cause an increase in the intracellular Ca^{2+} at electric fields significantly lower than those required to internalize Yo-Pro-1. The fact that no increase was detected in the absence of extracellular Ca^{2+} suggests that the observed increase in Ca^{2+} concentration is due to an uptake from the extracellular medium. One of the characteristic features of PRF treatments in the clinical practice is the large amount of bursts that are delivered and, according to our results, the delivery of multiple bursts significantly reduces the electric field amplitude required to observe a Ca^{2+} peak.

According to the electroporation literature, when square pulses are applied, the extent of membrane permeabilization and the recovery time depends on the duration of the applied pulses [41]. The shorter the pulses are, the smaller the pores that are created and the faster the membrane integrity is recovered. This effect is clearly seen when pulses in the nanosecond range are applied [42] where the electric field required to allow the entry of large molecules such as propidium iodide is significantly higher than the required to observe a Ca^{2+} influx. In the case of PRF, the sine waves in each burst can be regarded as a succession of short pulses (1 μs in each semi-cycle) with alternating polarity. In this scenario we would expect mostly small sized pores and a short membrane recovery time. In addition, pulses with alternating polarity are known to be less effective compared to monopolar pulses at

permeabilizing the membrane [43][44]. All this is aligned with, and may explain, our results that show that significantly larger electric fields are required in order to cause Yo-Pro-1 uptake by PRF bursts.

The temperature increase when delivering several bursts reached values of around 4.5 °C, thus, the possibility that the observed increase of Ca²⁺ was due to the cumulative temperature raise could not be ruled out. In addition, it must be noticed that PRF bursts, although not causing thermal damage to the tissues, generate large temperature spikes at each burst in a clinical set-up [28,29]. Since large temperature spikes also occurred in our experiments, a priori, we could not rule out either the possibility that those spikes caused the calcium influx. Indeed, it has been shown that the large temperature spikes generated by infrared laser pulses can cause the excitation of peripheral nerves [45], as well as a Ca²⁺ uptake and even Yo-Pro-1 internalization [46]. To investigate this possibility we looked at the effects of a single burst. The results in Figure 5 show that, for bursts with the same energy, the cell response largely depends on the waveform frequency. Note that, since the burst length was maintained in all experiments, the temperature evolution is expected to be the same for all frequencies. Therefore, if the Ca²⁺ influx was due to the temperature increase, or to the temperature spikes, the effect of the burst frequency would be null. This shows that the Ca²⁺ influx after a single burst was not associated to any thermal effect.

When delivering several bursts, the electric fields required to induce a Ca²⁺ peak and a Yo-Pro-1 uptake decreased. It may be argued that this was a consequence of the temperature increase during the delivery of these bursts. However, to the best of our knowledge there are no evidences in the literature that suggest that a temperature raise of around 4 °C, while still in the physiological range, can induce an uptake of Yo-Pro-1. In addition, the cumulative temperature increase was very similar over the entire imaging region. Therefore, if the Ca²⁺ influx was due to the temperature increase, we would have detected a large number of cells displaying a Ca²⁺ peak for electric fields below the measured E50 values.

The cell response dependence on the frequency and the extracellular conductivity suggests that the observed Ca²⁺ influx is related to a TMV dependent effect. Indeed, if we compare the results with the induced TMV calculated numerically, the trends observed experimentally are consistent with the results of the simulations. First, experimentally higher frequencies require higher electric fields to induce the same effect, which is consistent with the TMV dependence with frequency. Second, at 10 kHz the effects are very similar regardless of the medium conductivity, however, at 500 kHz the cells treated in a low conductivity medium required significantly larger electric fields to show the same responses. This is also consistent with the induced TMV dependence on the external conductivity.

All the above strongly supports that the Ca²⁺ influx observed in our experiments is dependent on the induced TMV. It could be hypothesized that such TMV related influx is related to voltage gated channels. However, it must be noted that the cells used in our experiments endogenously express very few voltage gated Ca²⁺ channels [47]. In fact, we have estimated the possible contribution of the voltage gated Ca²⁺ channels in our results assuming implausible extreme behaviors (see supplementary material) and we have concluded that the observed Ca²⁺ influx cannot be primarily attributed to transport through the ion channels. Therefore, we finally conclude that the most plausible pathway of the observed Ca²⁺ influx is associated to electroporation.

The effects of Ca²⁺ in cells have been extensively studied in the last decades and it is known that even a small amount of Ca²⁺ ions can trigger a wide variety of neuronal changes [48]. On the one hand, local increases in Ca²⁺ concentration can lead to alterations in synaptic function locally at the regions of Ca²⁺ influx. On the other hand, besides local effects, a Ca²⁺ influx can activate signaling pathways that affect the expression of several activity-regulated genes in neurons.

After in vivo PRF treatments several alterations in gene expression have been reported. Most of these alterations are consistent with a Ca^{2+} influx as is the case of c-fos [49], BDNF [50] and ATF3 [51]. In addition, an increase in the cytosolic Ca^{2+} concentration is consistent with the ultrastructural changes reported in axons after PRF exposure such as the disruption of neurofilaments [52] and changes in the morphology of mitochondria [53].

Electroporation was already suggested as being involved in the mechanism of action of PRF [29]. However, the suggested participation of electroporation was not related to Ca^{2+} . Instead, it was suggested a direct effect on neural conduction through a transient disruption of the membrane. Indeed, it is known that electroporation can transiently block neuronal conduction [54]. A recent study showed evidence of a long term depression effect after PRF treatments [23]. This finding is aligned with the results reported by Cahana et al. [55] which to the best of our knowledge is the only in vitro study on PRF effects available in the literature. In that study the authors showed that PRF causes a transient inhibition of evoked synaptic activity in hippocampal slice cultures. In both cases the reduction in the evoked synaptic activity that the authors attributed to a long term depression is also consistent with a conduction block caused by electroporation. Nevertheless, the hypothesis that PRF effects rely on a conduction block due to electroporation has two major flaws: first, it is inconsistent with the long lasting effects of PRF (several months) [4] and, second, the electric field required to block neuronal conduction through electroporation is very high compared to the electric fields generated in PRF treatments [28,29]. In contrast, what we propose is a "mild electroporation" phenomenon in which membrane permeability is increased during each PRF burst allowing Ca^{2+} ions to enter the cell. The effects of PRF would not be a direct consequence of membrane electroporation but an indirect consequence of the events and cell responses triggered by the massive ion influx.

Finally, it is worth noting an experimental observation regarding PRF treatments that, at first glance, would contradict the hypothesis that the mechanism of action of PRF treatments is based on an electroporation mediated calcium influx. PRF applied directly to nerves has shown to selectively affect small unmyelinated C fibers and spare larger and myelinated A- δ and A- β fibers [14]. In contrast, electroporation is expected to have a non-selective effect. This apparent contradiction with the electroporation hypotheses might be explained by the fact that the myelin sheath allowing Ca^{2+} entry is only present in a limited area (the nodes of Ranvier) in A- δ and A- β fibers while a larger area of C fibers can be permeabilized thus allowing a larger uptake of Ca^{2+} . Another possible explanation might be related to a higher capacity to recover normal conditions of larger fibers after an insult.

5. Conclusion

We showed that PRF bursts can cause a Ca^{2+} influx. Our results are consistent with the hypothesis that PRF causes a Ca^{2+} uptake mediated by a "mild" electroporation of the cell membrane. The results of this study may link the biological effects of PRF reported by other authors with a direct action of the electric fields in neurons.

Acknowledgments

This work was supported by the Ministry of Economy and Competitiveness of Spain through the grants TEC2014-52383-C3-2-R and SAF2014-52228-R. Antoni Ivorra gratefully acknowledges the financial support by ICREA under the ICREA Academia programme.

References

- [1] R. Lindner, M.E. Sluifjter, W. Schleinzer, Pulsed radiofrequency treatment of the lumbar medial branch for facet pain: A retrospective analysis, *Pain Med.* 7 (2006) 435–439. <https://doi.org/10.1111/j.1526-4637.2006.00175.x>.

- [2] J. Van Zundert, J. Patijn, A. Kessels, I. Lamé, H. van Suijlekom, M. van Kleef, Pulsed radiofrequency adjacent to the cervical dorsal root ganglion in chronic cervical radicular pain: A double blind sham controlled randomized clinical trial, *Pain*. 127 (2007) 173–182. <https://doi.org/10.1016/j.pain.2006.09.002>.
- [3] P.M. Schianchi, M.E. Sluijter, S.E. Balogh, S.A. Clinic, The Treatment of Joint Pain with Intra-articular Pulsed Radiofrequency, *Anesthesiol. Pain Med*. 3 (2013) 250–5. <https://doi.org/10.5812/aapm.10259>.
- [4] T. Vanneste, A. Van Lantschoot, K. Van Boxem, J. Van Zundert, Pulsed radiofrequency in chronic pain, *Curr. Opin. Anaesthesiol*. 30 (2017) 577–582. <https://doi.org/10.1097/ACO.0000000000000502>.
- [5] M.E. Sluijter, E.R. Cosman, W.B. Rittman, M. Van Kleef, The effects of pulsed radiofrequency fields applied to the dorsal root ganglion - a preliminary report, *Pain Clin*. 11 (1998) 109–117.
- [6] T.T. Simopoulos, J. Kraemer, J. V Nagda, M. Aner, Z.H. Bajwa, Response to pulsed and continuous radiofrequency lesioning of the dorsal root ganglion and segmental nerves in patients with chronic lumbar radicular pain., *Pain Physician*. 11 (2008) 137–144. <http://eutils.ncbi.nlm.nih.gov/entrez/eutils/elink.fcgi?dbfrom=pubmed&id=18354708&retmode=ef&cmd=prlinks%5Cnfile:///Users/myoung38/Documents/Papers2/Files/2008%5Cn11-3.pdf%5Cnpapers2://publication/uuid/1DE8D12A-B8ED-4B8F-9BF5-0770A0C76EB3>.
- [7] D. Vatansever, I. Tekin, I. Tuglu, K. Erbuyun, G. Ok, A Comparison of the Neuroablative Effects of Conventional and Pulsed Radiofrequency Techniques, *Clin. J. Pain*. 24 (2008) 717–724. <https://doi.org/10.1097/AJP.0b013e318173c27a>.
- [8] K. Tun, B. Cemil, A.G. Gurcay, E. Kaptanoglu, M.F. Sargon, I. Tekdemir, A. Comert, Y. Kanpolat, Ultrastructural evaluation of pulsed radiofrequency and conventional radiofrequency lesions in rat sciatic nerve, *Surg. Neurol*. 72 (2009) 496–500. <https://doi.org/10.1016/j.surneu.2008.11.016>.
- [9] M. Protasoni, M. Reguzzoni, S. Sangiorgi, C. Reverberi, E. Borsani, L.F. Rodella, A. Dario, G. Tomei, C. Dell’Orbo, Pulsed radiofrequency effects on the lumbar ganglion of the rat dorsal root: a morphological light and transmission electron microscopy study at acute stage, *Eur. Spine J*. 18 (2009) 473–478. <https://doi.org/10.1007/s00586-008-0870-z>.
- [10] A. Cahana, J. Van Zundert, L. Macrea, M. Van Kleef, M. Sluijter, Pulsed Radiofrequency: Current Clinical and Biological Literature Available, *Pain Med*. 7 (2006) 411–423. <https://doi.org/10.1111/j.1526-4637.2006.00148.x>.
- [11] N.H.L. Chua, K.C. Vissers, M.E. Sluijter, Pulsed radiofrequency treatment in interventional pain management: Mechanisms and potential indications - A review, *Acta Neurochir. (Wien)*. 153 (2011) 763–771. <https://doi.org/10.1007/s00701-010-0881-5>.
- [12] J. Hata, D. Perret-Karimi, C. DeSilva, D. Leung, N. Betesh, Z.D. Luo, S. Dawodu, K. Sinavsky, O.J. Stokes, S. English, Pulsed Radiofrequency Current in the Treatment of Pain, *Crit. Rev. Phys. Rehabil. Med*. 23 (2011) 213–240. <https://doi.org/10.1615/CritRevPhysRehabilMed.v23.i1-4.150>.
- [13] K. Ørstavik, C. Weidner, R. Schmidt, M. Schmelz, M. Hilliges, E. Jørum, H. Handwerker, E. Torebjörk, Pathological C-fibres in patients with a chronic painful condition., *Brain*. 126 (2003) 567–78. <https://doi.org/10.1093/brain/awg060>.

- [14] S. Erdine, A. Bilir, E.R. Cosman, E.R. Cosman Jr., Ultrastructural Changes in Axons Following Exposure to Pulsed Radiofrequency Fields, *Pain Pract.* 9 (2009) 407–417. <https://doi.org/10.1111/j.1533-2500.2009.00317.x>.
- [15] S. Choi, H.J. Choi, Y. Cheong, Y.J. Lim, H.K. Park, Internal-Specific Morphological Analysis of Sciatic Nerve Fibers in a Radiofrequency-Induced Animal Neuropathic Pain Model, *PLoS One.* 8 (2013). <https://doi.org/10.1371/journal.pone.0073913>.
- [16] S. Choi, H.J. Choi, Y. Cheong, S.H. Chung, H.K. Park, Y.J. Lim, Inflammatory responses and morphological changes of radiofrequency-induced rat sciatic nerve fibres, *Eur. J. Pain.* 18 (2014) 192–203. <https://doi.org/10.1002/j.1532-2149.2013.00391.x>.
- [17] J. Van Zundert, A.J. a de Louw, E. a J. Joosten, A.G.H. Kessels, W. Honig, P.J.W.C. Dederen, J.G. Veening, J.S.H. Vles, M. van Kleef, Pulsed and Continuous Radiofrequency Current Adjacent to the Cervical Dorsal Root Ganglion of the Rat Induces Late Cellular Activity in the Dorsal Horn, *Anesthesiology.* 102 (2005) 125–131. <https://doi.org/10.1097/00000542-200501000-00021>.
- [18] W. Hamann, S. Abou-Sherif, S. Thompson, S. Hall, Pulsed radiofrequency applied to dorsal root ganglia causes a selective increase in ATF3 in small neurons, *Eur. J. Pain.* 10 (2006) 171–176. <https://doi.org/10.1016/j.ejpain.2005.03.001>.
- [19] R. Vallejo, D.M. Tilley, J. Williams, S. Labak, L. Aliaga, R.M. Benyamin, Pulsed radiofrequency modulates pain regulatory gene expression along the nociceptive pathway., *Pain Physician.* 16 (2013) E601-13.
- [20] Y. Liu, Y. Feng, T. Zhang, Pulsed Radiofrequency Treatment Enhances Dorsal Root Ganglion Expression of Hyperpolarization-Activated Cyclic Nucleotide-Gated Channels in a Rat Model of Neuropathic Pain, *J. Mol. Neurosci.* 57 (2015) 97–105. <https://doi.org/10.1007/s12031-015-0582-x>.
- [21] Z. Jia, H. Ren, Q. Li, N. Ji, F. Luo, Pulsed radiofrequency reduced neuropathic pain behavior in rats associated with upregulation of GDNF expression, *Pain Physician.* 19 (2016) 49–58. <https://www.scopus.com/inward/record.uri?eid=2-s2.0-84961333959&partnerID=40&md5=5b551b401fcf78350df8490d45c31f9f>.
- [22] C.-C. Yeh, Z.-F. Wu, J.-C. Chen, C.-S. Wong, C.-J. Huang, J.-S. Wang, C.-C. Chien, Association between extracellular signal-regulated kinase expression and the anti-allodynic effect in rats with spared nerve injury by applying immediate pulsed radiofrequency, *BMC Anesthesiol.* 15 (2015) 92. <https://doi.org/10.1186/s12871-015-0071-3>.
- [23] R.-Y. Huang, C.-C. Liao, S.-Y. Tsai, C.-T. Yen, C.-W. Lin, T.-C. Chen, W.-T. Lin, C.-H. Chang, Y.-R. Wen, Rapid and Delayed Effects of Pulsed Radiofrequency on Neuropathic Pain: Electrophysiological, Molecular, and Behavioral Evidence Supporting Long-Term Depression., *Pain Physician.* 20 (2017) E269–E283. <http://www.ncbi.nlm.nih.gov/pubmed/28158164>.
- [24] T.Y. Tsong, Electroporation of cell membranes, *Biophys. J.* 60 (1991) 297–306. [https://doi.org/10.1016/S0006-3495\(91\)82054-9](https://doi.org/10.1016/S0006-3495(91)82054-9).
- [25] C. Chen, J. a Evans, M.P. Robinson, S.W. Smye, P. O'Toole, Measurement of the efficiency of cell membrane electroporation using pulsed ac fields., *Phys. Med. Biol.* 53 (2008) 4747–4757. <https://doi.org/10.1088/0031-9155/53/17/019>.
- [26] T. García-Sánchez, C. Merla, J. Fontaine, A. Muscat, L.M. Mir, Sine wave

- electropermeabilization reveals the frequency-dependent response of the biological membranes, *Biochim. Biophys. Acta - Biomembr.* 1860 (2018) 1022–1034. <https://doi.org/10.1016/j.bbamem.2018.01.018>.
- [27] T. Garcia-Sanchez, B. Mercadal, M. Polrot, A. Muscat, H. Sarnago, O. Lucia, L.M. Mir, Successful tumor Electrochemotherapy using Sine Waves, *IEEE Trans. Biomed. Eng.* (2019) 1–1. <https://doi.org/10.1109/TBME.2019.2928645>.
- [28] E. Ewertowska, B. Mercadal, V. Muñoz, A. Ivorra, M. Trujillo, E. Berjano, Effect of applied voltage, duration and repetition frequency of RF pulses for pain relief on temperature spikes and electrical field: a computer modelling study, *Int. J. Hyperth.* 6736 (2017) 1–10. <https://doi.org/10.1080/02656736.2017.1323122>.
- [29] E.R. Cosman, E.R. Cosman, Electric and Thermal Field Effects in Tissue Around Radiofrequency Electrodes, *Pain Med.* 6 (2005) 405–424. <https://doi.org/10.1111/j.1526-4637.2005.00076.x>.
- [30] T.B. Napotnik, Fluorescent Indicators of Membrane Permeabilization Due to Electroporation, in: *Handb. Electroporation*, Springer International Publishing, Cham, 2017: pp. 1305–1323. https://doi.org/10.1007/978-3-319-32886-7_133.
- [31] J. Schindelin, I. Arganda-Carreras, E. Frise, V. Kaynig, M. Longair, T. Pietzsch, S. Preibisch, C. Rueden, S. Saalfeld, B. Schmid, J.-Y.J.-Y. Tinevez, D.J. White, V. Hartenstein, K. Eliceiri, P. Tomancak, A. Cardona, K. Liceiri, P. Tomancak, C. A., Fiji: An open source platform for biological image analysis., *Nat. Methods.* 9 (2012) 676–682. <https://doi.org/10.1038/nmeth.2019.Fiji>.
- [32] C.A. Schneider, W.S. Rasband, K.W. Eliceiri, NIH Image to ImageJ: 25 years of image analysis., *Nat. Methods.* 9 (2012) 671–5. <https://doi.org/10.1038/nmeth.2089>.
- [33] R Core Team, R: A Language and Environment for Statistical Computing, (2014). <http://www.r-project.org/>.
- [34] R.F. Kubin, A.N. Fletcher, Fluorescence quantum yields of some rhodamine dyes, *J. Lumin.* 27 (1982) 455–462. [https://doi.org/10.1016/0022-2313\(82\)90045-X](https://doi.org/10.1016/0022-2313(82)90045-X).
- [35] J.J. Shah, M. Gaitan, J. Geist, Generalized temperature measurement equations for rhodamine B dye solution and its application to microfluidics, *Anal. Chem.* 81 (2009) 8260–8263. <https://doi.org/10.1021/ac901644w>.
- [36] B. Schmid, J. Schindelin, A. Cardona, M. Longair, M. Heisenberg, A high-level 3D visualization API for Java and ImageJ, *BMC Bioinformatics.* 11 (2010) 274. <https://doi.org/10.1186/1471-2105-11-274>.
- [37] J. Gimsa, T. Müller, T. Schnelle, G. Fuhr, Dielectric spectroscopy of single human erythrocytes at physiological ionic strength: dispersion of the cytoplasm, *Biophys. J.* 71 (1996) 495–506. [https://doi.org/10.1016/S0006-3495\(96\)79251-2](https://doi.org/10.1016/S0006-3495(96)79251-2).
- [38] M. Hibino, H. Itoh, K. Kinoshita, Time courses of cell electroporation as revealed by submicrosecond imaging of transmembrane potential, *Biophys. J.* 64 (1993) 1789–1800. [https://doi.org/10.1016/S0006-3495\(93\)81550-9](https://doi.org/10.1016/S0006-3495(93)81550-9).
- [39] R.W. Glaser, S.L. Leikin, L. V Chernomordik, V.F. Pastushenko, A.I. Sokirko, Reversible electrical breakdown of lipid bilayers: Formation and Evolution of Pores, *Biochim. Biophys.*

- Acta. 940 (1988) 275–287. [https://doi.org/10.1016/0005-2736\(88\)90202-7](https://doi.org/10.1016/0005-2736(88)90202-7).
- [40] T. Kotnik, D. Miklavčič, Theoretical Evaluation of Voltage Inducement on Internal Membranes of Biological Cells Exposed to Electric Fields, *Biophys. J.* 90 (2006) 480–491. <https://doi.org/10.1529/biophysj.105.070771>.
- [41] G. Saulis, R. Saule, Size of the pores created by an electric pulse: Microsecond vs millisecond pulses, *Biochim. Biophys. Acta - Biomembr.* 1818 (2012) 3032–3039. <https://doi.org/10.1016/j.bbamem.2012.06.018>.
- [42] T. Batista Napotnik, M. Reberšek, P.T. Vernier, B. Mali, D. Miklavčič, Effects of high voltage nanosecond electric pulses on eucaryotic cells (in vitro): A systematic review, *Bioelectrochemistry.* 110 (2016) 1–12. <https://doi.org/10.1016/j.bioelechem.2016.02.011>.
- [43] B.L. Ibey, J.C. Ullery, O.N. Pakhomova, C.C. Roth, I. Semenov, H.T. Beier, M. Tarango, S. Xiao, K.H. Schoenbach, A.G. Pakhomov, Bipolar nanosecond electric pulses are less efficient at electroporation and killing cells than monopolar pulses, *Biochem. Biophys. Res. Commun.* 443 (2014) 568–573. <https://doi.org/10.1016/j.bbrc.2013.12.004>.
- [44] A.G. Pakhomov, I. Semenov, S. Xiao, O.N. Pakhomova, B. Gregory, K.H. Schoenbach, J.C. Ullery, H.T. Beier, S.R. Rajulapati, B.L. Ibey, Cancellation of cellular responses to nanoelectroporation by reversing the stimulus polarity, *Cell. Mol. Life Sci.* 71 (2014) 4431–4441. <https://doi.org/10.1007/s00018-014-1626-z>.
- [45] J. Wells, C. Kao, P. Konrad, T. Milner, J. Kim, A. Mahadevan-Jansen, E.D. Jansen, Biophysical mechanisms of transient optical stimulation of peripheral nerve, *Biophys. J.* 93 (2007) 2567–2580. <https://doi.org/10.1529/biophysj.107.104786>.
- [46] H.T. Beier, G.P. Tolstykh, J.D. Musick, R.J. Thomas, B.L. Ibey, Plasma membrane nanoporation as a possible mechanism behind infrared excitation of cells, *J. Neural Eng.* 11 (2014). <https://doi.org/10.1088/1741-2560/11/6/066006>.
- [47] S. Berjukow, F. Döring, M. Froschmayr, M. Grabner, H. Glossmann, S. Hering, Endogenous calcium channels in human embryonic kidney (HEK293) cells., *Br. J. Pharmacol.* 118 (1996) 748–754. <https://doi.org/10.1111/j.1476-5381.1996.tb15463.x>.
- [48] S.W. Flavell, M.E. Greenberg, Signaling Mechanisms Linking Neuronal Activity to Gene Expression and Plasticity of the Nervous System, *Annu. Rev. Neurosci.* 31 (2008) 563–590. <https://doi.org/10.1146/annurev.neuro.31.060407.125631>.
- [49] M. Shimazawa, H. Hara, T. Watano, T. Sukamoto, Effects of Ca²⁺ channel blockers on cortical hypoperfusion and expression of c-Fos-like immunoreactivity after cortical spreading depression in rats, *Br. J. Pharmacol.* 115 (1995) 1359–1368. <https://doi.org/10.1111/j.1476-5381.1995.tb16624.x>.
- [50] X. Tao, S. Finkbeiner, D.B. Arnold, A.J. Shaywitz, M.E. Greenberg, Ca²⁺ influx regulates BDNF transcription by a CREB family transcription factor-dependent mechanism, *Neuron.* 20 (1998) 709–726. [https://doi.org/10.1016/S0896-6273\(00\)81010-7](https://doi.org/10.1016/S0896-6273(00)81010-7).
- [51] S.-J. Zhang, M. Zou, L. Lu, D. Lau, D.A.W. Ditzel, C. Delucinge-Vivier, Y. Aso, P. Descombes, H. Bading, Nuclear Calcium Signaling Controls Expression of a Large Gene Pool: Identification of a Gene Program for Acquired Neuroprotection Induced by Synaptic Activity, *PLoS Genet.* 5 (2009) e1000604. <https://doi.org/10.1371/journal.pgen.1000604>.

- [52] W.W. Schlaepfer, M.B. Hasler, Characterization of the calcium-induced disruption of neurofilaments in rat peripheral nerve, *Brain Res.* 168 (1979) 299–309. [https://doi.org/10.1016/0006-8993\(79\)90171-9](https://doi.org/10.1016/0006-8993(79)90171-9).
- [53] S. Deheshi, B. Dabiri, S. Fan, M. Tsang, G.L. Rintoul, Changes in mitochondrial morphology induced by calcium or rotenone in primary astrocytes occur predominantly through ros-mediated remodeling, *J. Neurochem.* 133 (2015) 684–699. <https://doi.org/10.1111/jnc.13090>.
- [54] G.S. Abramov, M. Bier, M. Capelli-Schellpfeffer, R.C. Lee, Alteration in sensory nerve function following electrical shock, *Burns.* 22 (1996) 602–606. [https://doi.org/10.1016/S0305-4179\(96\)00055-1](https://doi.org/10.1016/S0305-4179(96)00055-1).
- [55] A. Cahana, L. Vutskits, D. Muller, Acute differential modulation of synaptic transmission and cell survival during exposure to pulsed and continuous radiofrequency energy, *J. Pain.* 4 (2003) 197–202. [https://doi.org/10.1016/S1526-5900\(03\)00554-6](https://doi.org/10.1016/S1526-5900(03)00554-6).